HHS Public Access

Author manuscript

Dev Biol. Author manuscript; available in PMC 2017 January 01.

Published in final edited form as:

Dev Biol. 2016 January 1; 409(1): 152–165. doi:10.1016/j.ydbio.2015.11.004.

Neural crest requires *Impdh2* for development of the enteric nervous system, great vessels, and craniofacial skeleton

Jonathan I. Lake[1], **Marina Avetisyan**[1], **Albert G. Zimmermann**[2], and **Robert O. Heuckeroth**[3]

[1]Department of Pediatrics and Department of Developmental Regenerative and Stem Cell Biology, Washington University School of Medicine, 660 South Euclid Avenue, Box 8208, St. Louis, MO 63021, U.S.A

[2]Lineberger Comprehensive Cancer Center, University of North Carolina School of Medicine, 125 Mason Farm Rd, Chapel Hill, NC 27599

[3]Department of Pediatrics, Perelman School of Medicine at the University of Pennsylvania and the Children's Hospital of Philadelphia Research Institute, 3615 Civic Center Blvd, Philadelphia, PA 19104, U.S.A

Abstract

Mutations that impair the proliferation of enteric neural crest-derived cells (ENCDC) cause Hirschsprung disease, a potentially lethal birth defect where the enteric nervous system (ENS) is absent from distal bowel. Inosine 5′ monophosphate dehydrogenase (IMPDH) activity is essential for *de novo* GMP synthesis, and chemical inhibition of IMPDH induces Hirschsprung disease-like pathology in mouse models by reducing ENCDC proliferation. Two IMPDH isoforms are ubiquitously expressed in the embryo, but only IMPDH2 is required for life. To further understand the role of IMPDH2 in ENS and neural crest development, we characterized a conditional *Impdh2* mutant mouse. Deletion of *Impdh2* in the early neural crest using the Wnt1-Cre transgene produced defects in multiple neural crest derivatives including highly penetrant intestinal aganglionosis, agenesis of the craniofacial skeleton, and cardiac outflow tract and great vessel malformations. Analysis using a *Rosa26* reporter mouse suggested that some or all of the remaining ENS in *Impdh2* conditional-knockout animals was derived from cells that escaped Wnt1-Cre mediated DNA recombination. These data suggest that IMPDH2 mediated guanine nucleotide synthesis is essential for normal development of the ENS and other neural crest derivatives.

Corresponding Author: Robert O. Heuckeroth, M.D. Ph.D., Professor of Pediatrics, Perelman School of Medicine at the University of Pennsylvania, The Children's Hospital of Philadelphia, Research Institute, Abramson Research Center, 1116i, 3615 Civic Center Blvd, Philadelphia, PA 19104, Heuckerothr@email.chop.edu, Phone: 215-590-1209, FAX: 215-590-3324.

Author Contributions

J.I.L., M.A, and R.O.H. designed experiments to evaluate *Impdh2* mutant mice, analyzed the results, and wrote the manuscript. A.G.Z. designed the targeting vector and created the *Impdh2* mouse model. J.I.L. and M.A. performed the neural crest experiments.

Keywords

Neural crest; de novo purine synthesis; enteric nervous system

Introduction

The enteric nervous system (ENS) is a network of ganglia distributed throughout the digestive tract that autonomously controls motility, secretion, and blood flow (Furness, 2006). The ENS develops from migratory neural crest-derived cells that invade, migrate through, and colonize the nascent bowel while dividing rapidly, eventually reorganizing into discrete ganglia, and differentiating into glia or one of more than fifteen functional classes of neuron (Goldstein et al., 2013; Lake and Heuckeroth, 2013; Obermayr et al., 2013). A complete and functional ENS is required for life. Incomplete colonization of the bowel by ENS precursors results in Hirschsprung disease (HSCR), a life-threatening oligogenic birth defect where a segment of distal bowel is devoid of enteric neurons (aganglionosis). Bowel colonization critically requires that ENCDC proliferate efficiently (Lake et al., 2013; Simpson et al., 2007). For this reason, many of the mutations that cause HSCR impair ENS precursor proliferation or self-renewal (Amiel et al., 2008; Lake and Heuckeroth, 2013). Inhibition of ENCDC proliferation with the antimetabolite immunosuppressant mycophenolic acid (MPA) also causes aganglionosis in mice (Lake et al., 2013) and enhances the penetrance and phenotypic severity of mutations that model HSCR. MPA blocks the rate-limiting step of *de novo* guanine nucleotide synthesis by inhibiting inosine 5′ monophosphate dehydrogenase (IMPDH), a ubiquitous metabolic enzyme whose expression is relatively enriched in ENCDC (Lake et al., 2013). Prenatal MPA exposure in humans is also associated with a specific pattern of birth defects (Anderka et al., 2009), some of which are plausibly due to disruptions in neural crest development (Lin et al., 2011).

Relatively little is known about the developmental roles of IMPDH, which is present in two isoforms encoded by separate genes in vertebrates. *IMPDH2* is widely expressed and is enriched in activated lymphocytes, tumor cells, fetal tissues, and other proliferative cells (Zimmermann et al., 1995; Senda and Natsumeda, 1994; Nagai et al., 1992). Homozygous *Impdh2* deletion in mice results in early lethality prior to embryo implantation, while heterozygous deletion results in a subtle reduction in the IMPDH activity of splenic lymphocytes (Gu et al., 2000). *IMPDH1* is also ubiquitously expressed, but does not appear to be regulated by proliferative demand, and has a specialized but poorly-understood role in the retina (Aherne et al., 2004; Bowne et al., 2006; Gunter et al., 2008; Nagai et al., 1992; Zimmermann et al., 1996), where missense mutations in *IMPDH1* cause a form of autosomal dominant retinitis pigmentosa in humans. In mice, *Impdh1* is dispensable for life and its deletion results in a relatively mild retinal phenotype (Aherne et al., 2004; Gu et al., 2003) suggesting *Impdh2* is essential for early development.

Our previous experiments with the non-selective IMPDH inhibitor mycophenolic acid did not target IMPDH inhibition to neural crest derivatives, nor did they indicate whether IMPDH1 and IMPDH2 have redundant roles or whether one isoform is uniquely required for neural crest development. Since *Impdh1* homozygous mutant mice are viable and fertile

and thus must form a complete and functional ENS, we hypothesized that *Impdh2* is required within the neural-crest lineage for ENCDCs to proliferate efficiently and colonize the bowel. To further explore the role for this basic metabolic pathway in development, we deleted *Impdh2* in the early neural crest of mice using an $Impdh2^{loxP}$ allele and Wnt1-Cre transgene.

The Tg(Wnt1-cre)11Rth transgenic line (referred to as Wnt1-Cre), (Danielian et al., 1998) is a Cre-expressing line widely-used for tissue-specific recombination within the developing ENS and other neural crest derivatives. In this transgene, the Cre sequence is inserted into a *Wnt1* minigene construct between the endogenous promoter and a 5.5 kb downstream enhancer (Echelard et al., 1993). These elements confer an expression pattern nearly identical to endogenous *Wnt1* mRNA beginning in the developing midbrain and later extending, restricted to the closing neural folds and dorsal neural tube, cephalad into the telencephalon and caudad down the entire length of the neural tube (Echelard et al., 1994). While *Wnt1* expression is not maintained during neural crest delamination, Wnt1-Cre efficiently recombines the ancestors of all examined neural crest derivatives including the peripheral nervous system, adrenal medulla, great vessels, melanocytes (Jiang et al., 2000), craniofacial skeleton (Jiang et al., 2002), and the enteric nervous system (Lee et al., 2004).

Here we demonstrate that *Impdh2* expression is required in the neural crest for development of the craniofacial skeleton, cardiac outflow tract, and enteric nervous system. In the ENS, loss of *Impdh2* results in extensive bowel aganglionosis. Furthermore, ENCDC that do colonize the bowel in *Impdh2* conditional mutant mice are delayed and demonstrate incomplete Cre/loxP recombination, indicating a strong selective pressure against *Impdh2* deletion. Collectively these data support the need for de-novo guanine nucleotide synthesis and cell proliferation during neural crest development and are consistent with the hypothesis that IMPDH1 does not adequately supply metabolic guanine nucleotide needs for these neural crest-derived cell populations.

Materials and Methods

Impdh2 Gene Targeting

The pOSfrt-loxP vector (Provided by Randy Thresher, Lineberger Comprehensive Cancer Center Animal Models Core) containing a FRT-flanked positive selection marker (MC1-Neo) and a negative selection marker (PGK-TK) was used to assemble the *Impdh2* targeting construct from a 129/SV derived mouse genomic *Impdh2* clone (Agilent Lambda FIX II). A XbaI/XbaI fragment containing *Impdh2* exons 10–14 and 3′ flanking region (4.6 kb ‘long arm’) was filled-in using T4 DNA polymerase (Promega) and cloned into the PmeI site of pOSfrt-loxP using T4 DNA ligase (NEB) 3′ to the FRT-flanked MC1-Neo cassette. A second 3.5 kb fragment was synthesized by PCR using one primer located in intron 1 (5′ AAG GGT ACC CAT ATG TGA AGC AGG GGC AGG GGT TTA GAG G 3′) and a second loxP sequence-containing primer located in intron 9 (5′ CCG GGT ACC ATA ACT TCG TAT AAT GTA TGC TAT ACG AAG TTA TAG AGA TGC CAA GTC AGG CCT TGC C 3′). KpnI restriction sites at both ends of the amplified product were utilized to clone the fragment into the KpnI site of pOSfrt-loxP between the FRT-flanked MC1-Neo cassette and the 4.6 kb “long arm”. The entire PCR insert was sequenced and confirmed to be void of

mutations. To complete the targeting construct, a 3.3 kb XbaI/NdeI fragment containing the 5′ end of *Impdh2* (5′ flanking sequence through exon 1, 'short arm') was filled-in and ligated into the PmlI site of pOSfrt-loxP containing the other two fragments, between the PGK-TK gene and the FRT-flanked MC1-Neo cassette. Sequencing of the completed targeting vector (Figure S1) revealed that the most 5′ portion of this fragment was phage vector DNA located between *Impdh2* genomic sequences and the PGK-TK cassette, and that the homologous 'short arm' was 1.3 kb long.

Transfection and selection of E14TG2a (129/Ola) ES cells and generation of chimeras was performed by the Animal Models Core of the UNC-Lineberger Comprehensive Cancer Center. A total of 96 electroporated ES cell clones (A1-H12) were screened by PCR using the forward primer 5′-AACATGTCAGGAACCCTGCC-3′, located upstream and outside of the region of homologous recombination, and the reverse primer 5′-ACGCGTCACCTTAATATGC-3′ located in the Neo cassette using Takara LA Taq DNA Polymerase (Clontech Laboratories). Three PCR positive clones B3, C4 and D7 yielded a correctly sized 2206 bp product. The positive status of these clones were confirmed by two independent Southern blot analyses utilizing ES cell genomic DNA digested with the restriction enzymes XbaI and SalI, respectively. A 792 bp DNA fragment obtained from 129/Ola ES cell genomic DNA (spanning bp positions −772 through +20 relative to the translation start site and encompassing the *Impdh2* promoter through Exon 1) served as the Southern probe and was labeled using random priming (Prime-a-Gene, Promega). Southern blot analysis employing XbaI resulted in the expected 3502 bp and 1654 bp DNA fragments representing the WT and targeted IMPDH 2 alleles, respectively (Figure 1C). Southern blot analysis employing SalI resulted in 17312 bp and 12533 bp DNA fragments representing the WT and targeted IMPDH 2 alleles, respectively (not shown). A single correctly targeted ES cell clone, C4, was selected for microinjection, and the resulting agouti male chimeras were bred to C57Bl/6 females to accomplish germline transmission. The MC1-Neo cassette was excised by mating to Flp-recombinase expressing mice to produce the $Impdh2^{tm2Bmi}$ (referred to subsequently as $Impdh2^{loxP}$) allele.

Animals and Genotyping

Animal experiments were approved by the Washington University Animal Studies Committee, The Institutional Animal Use and Care Committee at The Children's Hospital of Philadelphia Research Institute, and the University of North Carolina – Chapel Hill's Institutional Animal Care and Use Committee. All mice were maintained on mixed genetic backgrounds with functional HPRT-mediated purine salvage. Since E14TG2a ES cells carry the $Hprt^{b\text{-}m3}$ null mutation, PCR was used to confirm that the $Impdh2^{loxP}$ strain did not carry $Hprt^{b\text{-}m3}$ (Lake et al., 2013) prior to experimental matings. Cre-mediated recombination of the $Impdh2^{loxP}$ allele results in a frameshift after codon 32 and a premature stop after codon 48, preventing expression of the catalytic domain. To produce a conventional knock-out allele, $Impdh2^{loxP/+}$ mice were bred to Tg(ACTB-cre)2Mrt/J "Actin-Cre" mice (Lewandoski et al., 1997 RRID:IMSR_JAX:003376) resulting in pups carrying a germline deletion: $Impdh2^{tm2.1Bmi}$ (referred to as $Impdh2^{Del}$). Actin-Cre was then removed through further breeding prior to experimental matings. $Impdh2^{loxP}$ mice were bred to $Gt(ROSA)26Sor^{tm1(EYFP)Cos}$ (Srinivas et al., 2001 RRID:IMSR_JAX:006148) mice

(referred to as *Rosa26*^{EYFP}) which permanently marks all Cre-expressing cells and their descendants with EYFP expression. *Impdh2*^{loxP} and *Impdh2*^{Del} mice were bred to Tg(Wnt1-cre)11Rth (Danielian et al., 1998 RRID:IMSR_JAX:003829) mice, (referred to as Wnt1-Cre), which drives loxP recombination in the entire neural crest and the dorsal tissues of the neural tube of the midbrain and hindbrain (Jiang et al., 2002). These strains were intercrossed as indicated using timed matings to produce Wnt1-Cre *Impdh2*$^{loxP/+}$ conditional heterozygotes (control animals) and the two conditional knockout genotypes, Wnt1-Cre *Impdh2*$^{loxP/loxP}$ and Wnt1-Cre *Impdh2*$^{loxP/Del}$, with and without the *Rosa26*^{EYFP} reporter.

The vaginal plug day was counted as embryonic day 0.5. For collection of fetal samples, dams were euthanized with CO_2 according to institutionally-approved procedures. Embryonic day 18.5 (E18.5) fetuses were euthanized by decapitation except for fetuses to be processed for bone and cartilage staining, which were anesthetized prior to immersion fixation. Tail DNA was prepared using the HotSHOT method (Truett et al., 2000) and genotyped using a previously described PCR genotyping protocol (Stratman et al., 2003). Genotyping reactions for Cre recombinase-containing transgenes and Rosa26^{EYFP} used previously described primers (Lake et al., 2013; Stratman et al., 2003). The *Impdh2*$^{+}$ and *Impdh2*^{loxP} alleles were genotyped using primer pair Impdh2-F: 5′GAC TAC CTG ATT AGC GGA GGC ACC TCT TAC3′ and Impdh–5FRTlox-R: 5′CAC GCT AAC ATA TTC CAC ATA TCC AGA GAA3′, producing a 320 bp band from the wild-type allele and a 450 bp band from the conditional allele. The *Impdh2*^{Del} allele was genotyped with primer pair Impdh2-F and Impdh–3lox-R: 5′CTG AAA GAC ACC TAT ACC AAG TCC ATA GCC3′ resulting in a 650 bp band indicating the presence of the deleted allele. All analyzed mice were hemizygous for the Wnt1-Cre transgene and heterozygous for *Rosa26*^{EYFP} if it was present.

Bone and Cartilage Staining

Simultaneous staining with alizarin red S and alcian blue was performed essentially as described in (McLeod, 1980). E18.5 mouse fetuses were fixed in 95% ethanol for two hours, after which skin and organs were removed and fixation was continued for one week. Samples were moved to acetone for two days and then stained for 3 days at 37 °C in 0.015% alcian blue (Sigma #A5268), 0.005% alizarin red S (Sigma #5533), 5% glacial acetic acid, and 70% ethanol. Samples were washed with water and rocked in a 1% KOH solution at room temperature until skeletons became visible after 48 hours. Samples were then passed through a graded series of 20–80% glycerol/1% KOH baths over the course of several weeks until tissues cleared. Skeletal preparations were stored and photographed in 100% glycerol.

Whole-mount Immunofluorescent Staining

Enteric neurons were labeled in E18.5 fetal mouse bowel using human ANNA–1 antiserum (A gift of Vanda Lennon, Mayo Clinic, RRID:AB_2313944), which stains the somas of all enteric neurons (Lennon, 1994) with the same pattern as the anti HuC/HuD monoclonal antibody used in previous studies (Lake et al., 2013). Fetal bowel was harvested, flushed with PBS, fixed with 4% paraformaldehyde in phosphate-buffered saline (PBS) for 30 minutes at room temperature, and then incubated in blocking solution for 1 hour at 37 °C: 5% normal goat serum (Jackson ImmunoResearch #005–000–121), 1% cold water fish-skin

gelatin (Sigma #G7765), 100 mM Glycine in Tris-buffered saline pH 7.5 with 1% Triton-X 100 (TBST). Samples were then incubated overnight at 4 °C in ANNA–1 antiserum diluted 1:2000 in ANNA–1 diluent (5% normal goat serum, 1% bovine serum albumin, and 0.2% sodium azide in PBS). Samples were washed 3 times with PBS and incubated with Alexa–594 conjugated goat anti-human secondary antibody (1:400, Life Technologies #A–11014, RRID:AB_10375428) at 37 °C for 1 hour in PBS. After 3 washes with PBS, samples with the *Rosa26*^{EYFP} reporter were incubated overnight at 4 °C with chicken anti-GFP (1:1000, Aves Labs #GFP–1020, RRID:AB_10000240) in blocking solution, washed 3 times with TBST, incubated for 1 hour at 37 °C with Alexa–488 conjugated goat-anti-chicken (1:400, Life Technologies #A–11039, RRID:AB_10563770), and washed 3 times with PBS.

Embryonic day 13.5 (E13.5) fetuses were pulse-labeled by maternal intraperitoneal bromodeoxyuridine (BrdU) injections (100 μg/gram body weight) with a one-hour chase. To label ENCDCs in EYFP-negative and some EYFP positive samples, a polyclonal rabbit antibody was used that was originally raised against SOX9 (Smith et al., 2005, rabbit anti-SoxE, RRID:AB_2491620) and reacts with the other Sox group E proteins, SOX8 and SOX10. SOX9 is not expressed in the neural crest at this time point and SOX8 and SOX10 are co-expressed in ENCDCs (Maka et al., 2005). Fetal bowel was harvested, processed, and stained for EYFP, cleaved-caspase 3 (Cell Signaling #9661, RRID:AB_2341188) or for SOXE exactly as described (Lake et al., 2013), except that rat anti-BrdU (1:400, BU1/75, Abcam #ab6326, RRID:AB_305426) and Alexa–594 conjugated donkey anti-rat (1:400, Life Technologies A–21209, RRID:AB_10562899) was used to visualize BrdU incorporation instead of a fluorophore-conjugated primary antibody. All samples were mounted on slides and visualized in 50% glycerol/PBS.

TUNEL Assay and Immunofluorescent Staining of Cryosections

Apoptosis was detected in 12 μm cryosections of E9.5 whole embryos using the *In Situ* Cell Detection Fluorescein Kit (Roche 11684795910) according to the manufacturer's instructions. Briefly, cryosections of fixed embryos were first treated with PBS containing 0.1% Triton X-100 for 2 minutes. Following three PBS rinses, cryosections were incubated in a TUNEL-Mix containing 90 μL TUNEL label and 10 μL TUNEL enzyme in the dark for 1 hour at 37 °C. Adult liver cryosections were included in each experiment as a positive control for TUNEL labeling. To perform immunofluorescence staining, cryosections were then blocked for 1 hour in 5% normal donkey serum (Jackson ImmunoResearch 017-000-121), incubated overnight at 4 °C in rabbit-anti-SOX E (1:300), washed three times with PBS, incubated for one hour with Alexa–594 conjugated donkey-anti-rabbit (1:400, Life Technologies A-21207), and washed three times with PBS before visualization in VECTASHIELD mounting medium with DAPI (Vector Laboratories H-1200).

Microscopy and Measurement

Photographs of whole fetuses, skeletal preparations, and hearts were acquired on an Olympus SZ–40 stereomicroscope. EYFP fluorescent micrographs of whole fetuses were acquired on a Nikon SMZ1500 stereomicroscope using a GFP-B epifluorescence filter. Measurements of colonization, aganglionosis and hypoganglionosis were conducted on an IX71 epifluorescence microscope guided by ANNA–1 staining at E18.5 or by SOXE and

EYFP staining at E13.5. Images of fluorescent whole-mount bowel were acquired as wide-field fluorescent micrographs on a Zeiss Axio Observer.Z1 or as multiple optical sections using either a Zeiss Apotome.2 structured illumination device or an Olympus FV1000 point-scanning confocal microscope. BrdU positivity within EYFP-positive cells was manually counted from confocal volumes. All optically sectioned samples are presented as maximum intensity projections through 20 micron-thick volumes unless otherwise indicated. Image processing was performed in ImageJ software (Schneider et al., 2012 RRID:nif-0000-30467) and was limited to stitching of multiple fields (Preibisch et al., 2009), rotation, cropping, uniform brightness and contrast adjustments, and maximum intensity projection of volumes, with the exception of EYFP fluorescent micrographs of whole E13.5 fetuses, which were subjected to local contrast enhancement using contrast limited adaptive histogram equalization (CLAHE) (Schindelin et al., 2012) to improve the contrast of EYFP-containing tissue.

Statistical Analysis

Statistical tests were performed using the R software package (R. Core Team, 2012 RRID:nif-0000-10474). Student's *t* test was used to compare E13.5 bowel colonization and rates of BrdU incorporation within ENCDCs. Multiple comparison adjustments were performed with the Holm-Boniferroni method based on the number of planned comparisons.

Results

Impdh2 deletion in the neural crest results in craniofacial and cardiac defects

Guanine nucleotides can be produced either *de novo* via IMPDH1/IMPDH2 or by the purine salvage pathway. To determine whether *Impdh2* is required within the neural crest lineage for ENS development or whether *Impdh1* and/or purine salvage from adjacent tissue could provide adequate GMP once embryonic lethality was bypassed, we used the Wnt1-Cre transgene to delete a conditional $Impdh2^{loxP}$ allele (Figure 1) in the early neural crest. As expected, both $Impdh2^{loxP/loxP}$ and $Impdh2^{loxP/Del}$ mice lacking Wnt1-Cre survived to adulthood and were fertile. While Wnt1-Cre $Impdh2^{loxP/+}$ mice appeared normal, Wnt1-Cre $Impdh2^{loxP/loxP}$ mice did not survive after birth, though they did develop to term. At E18.5, Wnt1-Cre $Impdh2^{loxP/loxP}$ fetuses had profound malformations of the anterior head (Figure 2A,E) including a near-total absence of the jaw and a protruding brain that was not covered by bone. Eyes were sometimes open, and ear pinnae were rudimentary. Bone and cartilage staining revealed that most skeletal structures anterior to the parietal (dorsal) or basisphenoid (ventral) bones were reduced or ablated, and the remaining structures consisted of irregular spicules of bone and cartilage (Figure 2B–D,F–H). Notably, these structures are normally neural crest-derived. Several posterior elements of the skull that are neural crest-derived are also reduced or missing in Wnt1-Cre $Impdh2^{loxP/loxP}$ fetuses, such as the interparietal bone and tympanic rings (Huang et al., 2010; Jiang et al., 2002). Because neural crest also contributes to portions of several neck and shoulder bones (Matsuoka et al. 2005), we further inspected the clavicle, sternum, scapular spine, and spinous process of the cervical vertebrae in Wnt1-Cre $Impdh2^{loxP/loxP}$ fetuses, but found no gross abnormalities in these structures (Figure 2I–N). Since our previous experiments with IMPDH inhibition also revealed heart defects in exposed fetuses, we examined hearts at E18.5 using dye injection into the left

ventricle and observed outflow tract and great vessel defects in 4 of 8 Wnt1-Cre *Impdh2*$^{loxP/loxP}$ fetuses (Figure 2O–Q).

Neural crest-specific deletion of *Impdh2* results in bowel aganglionosis

Examination of enteric neurons in E18.5 fetal bowel using ANNA–1 (anti-HuC/HuD) staining revealed normal colonization in Wnt1-Cre *Impdh2*$^{loxP/+}$ fetuses while deletion of *Impdh2* in the neural crest of Wnt1-Cre *Impdh2*$^{loxP/loxP}$ fetuses resulted in severe defects of the ENS including highly-penetrant aganglionosis of variable length (Figure 3A–C) ranging from very short colonic aganglionosis to total intestinal aganglionosis. In bowels that contained normally-innervated regions, those regions were always oral to hypoganglionic and aganglionic regions, strongly suggesting that *Impdh2* deletion causes a vagal ENCDC colonization defect. Some isolated enteric neurons were also found in the walls of otherwise aganglionic colons and are possibly of sacral neural crest origin. We were concerned that the variable phenotype seen in the conditional knockout was due to the presence of two “floxed” alleles of *Impdh*, resulting in either incomplete recombination or a failure to reduce IMPDH2 protein levels quickly enough to produce a complete phenotype in the ENS. To address this concern, we converted one copy of *Impdh2*^{loxP} to the deleted allele *Impdh2*^{Del} in the germline and examined the phenotype of Wnt1-Cre *Impdh2*$^{loxP/Del}$ fetuses. This configuration requires only a single recombination event to delete *Impdh2*. This strategy greatly increased the severity of the ENS phenotype. (Figure 3A,D).

Impdh2 deleted ENCDCs colonize the bowel abnormally

Because of the distal aganglionosis apparent at E18.5, we examined the effects of *Impdh2* deletion as the ENCDC migration process nears completion at E13.5 using a mouse strain that expresses EYFP after Cre-induced DNA recombination, *Rosa26*^{EYFP}. The craniofacial defects that result from *Impdh2* deletion were readily apparent at E13.5. While lineage-marked EYFP+ cranial neural crest cells did migrate to the expected regions of the anterior head in Wnt1-Cre *Impdh2*$^{loxP/loxP}$ and Wnt1-Cre *Rosa26*^{EYFP} *Impdh2*$^{loxP/Del}$ fetuses, the resulting structures were abnormal in Wnt1-Cre *Rosa26*^{EYFP} *Impdh2*$^{loxP/loxP}$ embryos and the pharyngeal arches were almost entirely absent in the *Impdh2*$^{loxP/Del}$ genotype (Figure 4A,C,E). In the ENS, Wnt1-Cre *Impdh2*$^{loxP/+}$ colons were uniformly colonized at E13.5 as indicated by EYFP fluorescence or SOXE staining. In contrast, both Wnt1-Cre *Impdh2*$^{loxP/loxP}$ and Wnt1-Cre *Impdh2*$^{loxP/Del}$ genotypes showed severe colonization defects at E13.5 (Figure 4B,D,F–G) and colonization in the Wnt1-Cre *Impdh2*$^{loxP/Del}$ genotype was slightly but significantly reduced relative to Wnt1-Cre *Impdh2*$^{loxP/loxP}$ (Figure 4G). The structure of the proximal colonized regions of the ENS was also abnormal in both conditional knockout genotypes. In *Impdh2*$^{loxP/+}$ fetuses, the ENCDCs immediately behind the wavefront were organized into chains of cells (Figure 4B), quickly transitioning into a high-density network more proximally. In contrast, Wnt1-Cre *Impdh2*$^{loxP/loxP}$ and Wnt1-Cre *Impdh2*$^{loxP/Del}$ bowel contained long stretches of low-density ENCDC strands and even isolated ENCDCs (Figure 4D,F). Notably, the proximal colonized areas of E18.5 bowel appeared essentially normal (Figure 3), indicating that these sparse strands of ENCDCs did expand between E13.5 and E18.5 to populate the colonized regions of the proximal bowel. In an effort to determine the fate of *Impdh2*-deficient ENCDCs, we measured DNA synthesis and apoptosis at E13.5 using BrdU labeling and cleaved-caspase 3 staining. We did

not detect significant numbers of cleaved-caspase 3 reactive ENCDCs of any genotype and found that BrdU incorporation in the EYFP-positive cells of E13.5 *Impdh2*$^{loxP/Del}$ bowel was not significantly reduced relative to EYFP-positive cells at the migration wavefront in *Impdh2*$^{loxP/+}$ fetuses (Figure 5). Additionally, analysis of cell death using TUNEL assay at E9.5, an age when vagal neural crest progenitors begin invading the proximal bowel, also revealed no significant apoptosis in mice of any genotype (Figure 6).

Wnt1-Cre incompletely recombines the *Rosa26*^{EYFP} reporter in the ENS of *Impdh2* conditional knockouts

E18.5 fetuses that also carried the *Rosa26*^{EYFP} reporter displayed an unexpected phenotype. In Wnt1-Cre *Impdh2*$^{loxP/+}$ bowel (N=4 EYFP-positive samples) stained for both ANNA-1 and EYFP, all neurons were EYFP-positive (Figure 7A), as expected given the Wnt1-Cre fate map (Jiang et al., 2002). However, in every *Impdh2*$^{loxP/loxP}$ *Rosa26*^{EYFP} fetus (N=3 EYFP-positive samples), mixtures of varying numbers of EYFP-positive and EYFP-negative neurons were clearly visible (Figure 7B–C). The degree of incomplete recombination varied both between animals and between regions of a single bowel, reflecting the clonal mixing that occurs during ENS development (Binder et al., 2012; Rothman et al., 1993; Young and Newgreen, 2001). Similarly, when we examined Wnt1-Cre *Impdh2*$^{loxP/+}$ and Wnt1-Cre *Impdh2*$^{loxP/Del}$ bowels carrying the *Rosa26*^{EYFP} reporter at E13.5 and stained for SOXE and EYFP, we observed many EYFP-negative ENCDCs in the *Impdh2*$^{loxP/Del}$ fetuses (2 of 4 embryos, Figure 7D–E). After searching the colonized regions of Wnt1-Cre *Impdh2*$^{loxP/+}$ bowels marked by EYFP (N=6), we found only a few scattered EYFP-negative SOXE-positive ENCDCs in a single embryo (Figure 7E), indicating that while Wnt1-Cre mediated recombination in the ENS is highly efficient, it is not universal, and that the degree of incomplete labeling for EYFP is influenced by the *Impdh2* genotype.

Discussion

A neural-crest autonomous requirement for *Impdh2*

Deletion of *Impdh2* in the early neural crest results in craniofacial defects including near-total ablation of skull structures derived from the neural crest (Chai et al., 2000; Jiang et al., 2002). This includes the skeleton anterior to the basisphenoid and parietal bones as well as the tympanic rings and the interparietal bone in the posterior skull (Figure 2). Bones in the neck and shoulder region known to receive neural crest contributions (Matsuoka et al. 2005) appeared grossly normal. Since these bones are only partially composed of neural crest derived cells, it is possible that subtle defects are present that could not be detected with the bone and cartilage staining performed. Alternatively, mesodermal progenitors may be able to compensate for the lack of neural crest derived cells in these structures.

Conditional *Impdh2* knockout fetuses also demonstrated cardiac outflow tract and great vessel defects. These phenotypes bear a striking resemblance to the pan-neural crest defects that result from experimental ablation of the Wnt1-Cre fate map using Cre recombinase-triggered expression of diphtheria toxin fragment-A (Olaopa et al., 2011) or HSV-Tk followed by ganciclovir treatment (Porras and Brown, 2008), which suggests that neural crest derivatives lacking *Impdh2* fail to expand, survive, or differentiate properly. Taken

together with the catastrophic results of *Impdh2* deletion in the ENS, these results reinforce our previous findings that global IMPDH inhibition results in cardiac and ENS defects (Lake et al., 2013). However, our previous work could not separate the effects of IMPDH inhibition on ENCDCs and non-neural crest tissues such as the bowel mesenchyme, which manifested as global growth restriction and reduced intestinal length in exposed fetuses. The current experiments clearly show that *Impdh2* is required in ENCDCs and other neural crest derivatives, and that the resulting ENS defects occur in the context of an entirely normal bowel microenvironment. Moreover, guanine salvage from this normal neighboring tissue and any residual GMP synthesis by IMPDH1 cannot compensate for the loss of IMPDH2.

Incomplete recombination in conditional deletion of *Impdh2*

The aganglionosis observed in *Impdh2* conditional knockout bowel demonstrates the necessity of IMPDH2 for ENS development, while the incomplete recombination seen in the ENS (Figure 7) of these fetuses provides indirect evidence that loss of *Impdh2* dramatically reduces the ability of neural crest-derived cells to populate fetal bowel. The Wnt1-Cre transgene has been used extensively to delete genes in and mark the cells of the ENS (Zehir et al., 2010; Fuchs et al., 2009; Okamura and Saga, 2008; Van de Putte et al., 2007), and we are unaware of any previous instances where incomplete recombination has been demonstrated in Wnt1-Cre mice, although it has been suggested that it may account for some otherwise contradictory results (D'Autréaux et al., 2007; Hendershot et al., 2007). Indeed, we observed only rare instances of incomplete recombination of the EYFP reporter in E13.5 $Impdh2^{loxP/+}$ $Rosa26^{EYFP}$ fetuses (Figure 7), suggesting that Cre-induced recombination is nearly complete in the ENS of Wnt1-Cre mice. The $Impdh2^{loxP/loxP}$ conditional knockout, on the other hand, shows clear evidence of incomplete recombination of the *Rosa26* reporter. Since each Cre-catalyzed recombination event is independent, when reporter recombination is incomplete we can no longer assert with confidence that every EYFP-positive cell has recombined the gene of interest. Because the Wnt1-Cre transgene is very efficient in conditional heterozygotes, we suspected that $Impdh2^{loxP/loxP}$ cells escaping recombination had a strong selective advantage early in neural crest development, leading to their overrepresentation in the ENS of conditional knockout fetuses. We also suspected that incomplete deletion of *Impdh2* could account for the variability in ENS phenotype. Since the *Impdh2* allele used in this study lacks an internal recombination reporter and all available anti-IMPDH antibodies suitable for immunohistochemistry lack specificity for IMPDH2, we attempted to circumvent this problem by using the $Impdh2^{loxP/Del}$ $Rosa26^{EYFP}$ genotype, reasoning that reducing the number of required recombination events from 3 to 2 might make both deletion and lineage marking more uniform. However, examination of the ENCDC population indicates that this was not entirely successful, since many SOXE-positive cells in $Impdh2^{loxP/Del}$ $Rosa26^{EYFP}$ bowels still escaped recombination at the *Rosa26* locus.

Using the $Impdh2^{loxP/Del}$ genotype likely increased *Impdh2* deletion efficiency and reduced the number of proliferation-competent cells entering the bowel, since the migration phenotype in $Impdh2^{loxP/Del}$ embryos at E13.5 was significantly worse than in mice with the $Impdh^{LoxP/LoxP}$ genotype and ENCDC migration depends largely on population size and proliferation (Barlow et al., 2008; Simpson et al., 2007). The relatively normal BrdU

labeling index in Wnt1-Cre *Impdh2*$^{loxP/Del}$ ENCDCs is also easily accounted for if the ENCDCs that do colonize the bowel in *Impdh* conditional mutant mice have preferentially not undergone recombination at the *Impdh2* locus despite sporadically recombining the *Rosa26*^{EYFP} reporter.

Incomplete lineage labeling is an inherent hazard of experiments that use separate target and reporter alleles. However, independent recombination of multiple loci does not necessarily explain why the *Impdh2*$^{loxP/Del}$ *Rosa26*^{EYFP} genotype produced obviously incomplete lineage labeling while the *Impdh2*$^{loxP/+}$ *Rosa26*^{EYFP} genotype, containing the same number of loxP-flanked recombination targets (two), produced an almost perfectly labeled ENS.

An alternative explanation for the unlabeled neural-crest derivatives is that the unlabeled cells might comprise a separate sublineage of ENCDCs that does not express the Wnt1-Cre transgene, and expands in reaction to depletion of surrounding ENCDCs. This possibility is important to consider because the existence of such a subpopulation could imply a currently unappreciated early specification or lineage restriction within the enteric neural crest and because heterogeneity in Wnt1-Cre expression has far-reaching consequences for interpreting the many experiments performed using this system. However, the near-total (far fewer than 1 in 1000 cells escape in control fetuses) labeling of all fetal and term ENS cells in *Impdh2*$^{loxP/+}$ animals is inconsistent with a distinct lineage, unless it normally contributes vanishingly few cells to the ENS. In contrast, a more numerous distinct ENS lineage has been described that normally comprises about 15% of ENCDCs and is defined by non-expression of a Nestin-Cre transgene. (Lei and Howard, 2011). This lineage increases its proliferation in reaction to the deletion of Hand2 (a transcription factor required for multiple aspects of ENS development) within the remaining 85% of ENCDCs (which express Nestin-Cre) and is also distinguished as a unique linage by preferentially generating neurons rather than glia, in contrast to other ENCDCs. Similarly, when *Foxd3* (a transcription factor required for neural-crest cell self-renewal) is deleted by a Ednrb-iCre (codon optimized Cre) transgene, ENCDCs that do not express the Ednrb-iCre transgene (normally comprising about 5% of p75+ cells) preferentially expand to compensate for absent recombined cells (Mundell et al., 2012). In the latter case, it is not clear whether this population represents a lineage with distinct properties or is the effect of variegated transgene expression.

Finally, differences in efficiency of Cre/loxP-mediated recombination between the *Impdh2* and *Rosa26* loci should be considered as a possible source of unlabeled neural crest derivatives. Efficiency of intramolecular Cre-mediated recombination is known to be reduced with increasing length between loxP sites (Wang et al., 2009; Zheng et al., 2000), but the sizes of the flanked region in *Impdh2* (3.5 kb) and Rosa26EYFP (2.8 kb) do not differ enough to skew recombination significantly. It is also known that different genomic loci have different efficiencies of recombination due to chromatin state, base composition, or other factors (Hara-Kaonga et al., 2006; Vooijs et al., 2001). Again, it is difficult to explain with this framework why unlabeled enteric neurons and ENCDCs would be more numerous in the *Impdh2*$^{loxP/loxP}$ and *Impdh2*$^{loxP/Del}$ genotypes.

Because expansion of the rare ENCDCs that escape recombination most parsimoniously explains the increased number of EYFP negative ENCDCs in the *Impdh2*$^{loxP/loxP}$ and

Impdh2$^{loxP/Del}$ genotypes and accounts for the lack of a proliferation defect in EYFP-labeled cells, we favor this interpretation.

Fate of ENCDCs in *Impdh2* conditional mutant fetuses

Consistent with results from mice treated with the IMPDH inhibitor MPA (Lake et al., 2013), we saw no increase in apoptosis of ENCDCs in *Impdh2* conditional mutants, either at E9.5 (Figure 6) or E13.5. This suggests that *Impdh2* depletion does not result in increased progenitor or ENCDC cell death, at least not through canonical apoptosis. It is however possible that at E9.5, progenitors are not yet fully IMPDH2 or guanine nucleotide depleted, and that increased apoptosis occurs in the time window between the two sampled time points (i.e. between E9.5 and E13.5).

Our data also suggest that there is ongoing ENCDC proliferation in conditional *Impdh2* mutant bowel between E13.5 and E18.5 since the bowel is more densely colonized by ENCDC at the later time point (Figures 3 and 4). This observation supports the idea that the sparsely colonized ENS network in fetal bowel is made up of “fugitive” ENCDCs whose ancestors escaped recombination and that these cells adaptively expand to fill the underpopulated bowel (Natarajan et al., 1999). To our knowledge, it is not known how long CRE activity from the Wnt1-Cre transgene lasts in the migratory neural crest. Expression of a similar Tg(Wnt1-LacZ) transgene in the developing ENS was lost after E11.5 (Kapur, 2000), suggesting that the rare ENCDC that had not yet recombined at that time would permanently escape Cre-mediated DNA recombination. It is also possible that non-recombined cells support some degree of migration of *Impdh2*-deleted cells through the bowel, since ENCDCs clones mix extensively and non-cell autonomous rescue of ENCDC migration occurs in aggregation chimeras (Kapur et al., 1996, 1995) and in tissue culture (Lake et al., 2013). In the absence of a method to directly detect *Impdh2* recombination on a cell-by-cell basis, we cannot determine if all ENCDC that colonize the bowel in mutant mice retain IMPDH2 expression.

In the absence of detectable proliferation defects or the induction of cell death, it is not obvious why impaired colonization of the bowel by ENCDC occurs. However, our data suggest that *Impdh2* deletion dramatically reduces the ability of ENCDCs to colonize fetal bowel. The small number of ENCDCs that remain replication and migration competent because they fail to recombine the *Impdh2* locus (< 1:1000 in Wnt1-Cre reporter lines), would need to divide and migrate very rapidly to produce a normal ENS before the bowel microenvironment becomes nonpermissive to further colonization (Hotta et al., 2010). As other studies have shown, reducing the number of ENCDCs that enter the bowel (Barlow et al., 2008) is sufficient to cause aganglionosis and artificially reducing the density of ENCDCs impairs their migration (Young et al., 2004) even if the remaining ENCDCs are healthy. This can account for the failure of the remaining ENCDCs to colonize the distal portions of the bowel. One notable exception to this is in *Tcof1*$^{+/-}$ haploinsufficient fetuses, where even very severe reductions in the number of ENCDCs entering the bowel are completely compensated for by a combination of increased ENCDC proliferation, decreased enteric neuron differentiation, and impaired microenvironment maturation (Barlow et al., 2012). In the case of *Impdh2* neural-crest specific deletion, aganglionosis results despite

apparent compensatory ENCDC proliferation from incompletely recombined cells, probably because bowel mesenchyme becomes inhospitable for further ENCDC proliferation and migration as development proceeds..

Unexpectedly, there appears to be less bowel colonization at E18.5 than at E13.5 in *Impdh2*$^{loxP/Del}$ mice (Figures 3, 4). Since we did not detect increased ENCDC apoptosis in mutant embryos at E13.5, this apparent regression might be explained by the dramatic lengthening of the midgut (post-ampullary small bowel) relative to the foregut (pre-ampullary small bowel) between E13.5 and E18.5. It is also possible that either apoptotic or non-apoptotic, non-necrotic cell death (Uesaka and Enomoto, 2010) occurs in ENCDCs at any time between E13.5 and E18.5 and was not detected due to event rarity or the time chosen for sampling. Alternatively, the nascent ENCDCs in the most distal region of colonized bowel could preferentially differentiate into glia. This would be difficult to detect, since extrinsic nerve fibers present in aganglionic regions carry their own Schwann cells which are indistinguishable from intrinsic enteric glia by immunohistochemical markers.

Conclusions

Taken together with our prior study demonstrating that chemical inhibition of IMPDH results in aganglionosis by reducing ENCDC proliferation (Lake et al., 2013), these experiments identify IMPDH2 as uniquely required for the development of the ENS. This is especially interesting since human genetic studies have independently identified a risk locus at 3p21 in Hirschsprung disease (Gabriel et al., 2002), and the *IMPDH2* gene is located at 3p21. In that analysis, the 3p21 risk allele appeared to enhance the effect of *RET* mutations, the primary causative mutation in most cases of Hirschsprung disease (Amiel et al., 2008). A subsequent study has mapped this risk locus to an interval 0.6 megabases from *IMPDH2* (Garcia-Barceló et al., 2008). Other modifier mutations are well-appreciated contributors to Hirschsprung disease (Carrasquillo et al., 2002; de Pontual et al., 2007; Garcia-Barcelo et al., 2009), and future studies will investigate whether known (Wang et al., 2007) or novel genetic variation in human *IMPDH2* is associated with Hirschsprung disease.

Because IMPDH inhibition impairs ENS development and the *Impdh2* gene is indispensable for embryonic survival, we examined whether *Impdh2* is required in the neural crest lineage for its proper development. Wnt1-Cre-mediated deletion of *Impdh2* resulted in severe craniofacial and heart defects, as well as extensive aganglionosis of the ENS. During initial ENS development, ENCDC colonization in conditional knockout fetuses was impaired and the remaining colonized regions were abnormally hypocellular. Furthermore, both the developing and definitive ENS showed evidence of incomplete recombination that was specific to the conditional knockout genotype, demonstrating that *Impdh2* deletion is strongly selected against in the neural crest-derived cells that eventually become the ENS. These results confirm a critical role for de novo guanine nucleotide synthesis and IMPDH2 in the neural crest lineage, and indicate that IMPDH1 and the salvage pathway cannot compensate for IMPDH2 loss even when other tissues in the developing embryo are normal.

Supplementary Material

Refer to Web version on PubMed Central for supplementary material.

Acknowledgments

The authors thank Sanjay Jain for providing Actin-Cre mice, the Mouse Genetics Core (http://mgc.wustl.edu) for mutant mouse line maintenance, Vanda Lennon for human ANNA-1 serum, and Craig Smith for the rabbit anti-SoxE antibody. Ming Fu, Hongtao Wang, Elizabeth Wright-Jin, Ellen Merrick Schill, Shahriyar Majidi and Rajarshi Sengupta provided help and support. The *Impdh2*^{loxP} mouse model generated in the laboratory of Beverly S. Mitchell (Stanford University) in collaboration with the Lineberger Comprehensive Cancer Center Animal Models Core was graciously provided by Dr. Mitchell. This work was supported by the Irma and Norman Braman Endowment (R.O.H.), The Suzi and Scott Lustgarten GI Motility Center Endowment (R.O.H), The Children's Hospital of Philadelphia Research Institute (R.O.H.), Children's Discovery Institute of Washington University and St. Louis Children's Hospital (R.O.H., grant nos. CH-II-1008-123 and CH-II-2010-390), NIH grants RO1 DK087715 and RO1 DK057038 (R.O.H.), a Burroughs Wellcome Fund Clinical Scientist Award in Translational Research (R.O.H., grant no. 1008525), and NIH grant R01-CA64192 (Dr. Beverly Mitchell). Jonathan Lake was supported by a National Research Science Award – Medical Scientist NIH T32 GM007200.

References

Aherne A, Kennan A, Kenna PF, McNally N, Lloyd DG, Alberts IL, Kiang AS, Humphries MM, Ayuso C, Engel PC, Gu JJ, Mitchell BS, Farrar GJ, Humphries P. On the molecular pathology of neurodegeneration in IMPDH1-based retinitis pigmentosa. Hum Mol Genet. 2004; 13:641–650.10.1093/hmg/ddh061 [PubMed: 14981049]

Amiel J, Sproat-Emison E, Garcia-Barcelo M, Lantieri F, Burzynski G, Borrego S, Pelet A, Arnold S, Miao X, Griseri P, Brooks AS, Antinolo G, de Pontual L, Clement-Ziza M, Munnich A, Kashuk C, West K, Wong KKY, Lyonnet S, Chakravarti A, Tam PKH, Ceccherini I, Hofstra RMW, Fernandez R. Hirschsprung disease, associated syndromes and genetics: a review. J Med Genet. 2008; 45:1–14.10.1136/jmg.2007.053959 [PubMed: 17965226]

Anderka MT, Lin AE, Abuelo DN, Mitchell AA, Rasmussen SA. Reviewing the evidence for mycophenolate mofetil as a new teratogen: Case report and review of the literature. Am J Med Genet A. 2009; 149A:1241–1248.10.1002/ajmg.a.32685 [PubMed: 19441125]

Barlow AJ, Dixon J, Dixon MJ, Trainor PA. Balancing neural crest cell intrinsic processes with those of the microenvironment in Tcof1 haploinsufficient mice enables complete enteric nervous system formation. Hum Mol Genet. 2012; 21:1782–1793.10.1093/hmg/ddr611 [PubMed: 22228097]

Barlow AJ, Wallace AS, Thapar N, Burns AJ. Critical numbers of neural crest cells are required in the pathways from the neural tube to the foregut to ensure complete enteric nervous system formation. Development. 2008; 135:1681–1691.10.1242/dev.017418 [PubMed: 18385256]

Binder BJ, Landman KA, Newgreen DF, Simkin JE, Takahashi Y, Zhang D. Spatial Analysis of Multi-species Exclusion Processes: Application to Neural Crest Cell Migration in the Embryonic Gut. Bull Math Biol. 2012; 74:474–490.10.1007/s11538-011-9703-z [PubMed: 22108739]

Bowne SJ, Liu Q, Sullivan LS, Zhu J, Spellicy CJ, Rickman CB, Pierce EA, Daiger SP. Why Do Mutations in the Ubiquitously Expressed Housekeeping Gene IMPDH1 Cause Retina-Specific Photoreceptor Degeneration? Invest Ophthalmol Vis Sci. 2006; 47:3754–3765.10.1167/iovs.06-0207 [PubMed: 16936083]

Carrasquillo MM, McCallion AS, Puffenberger EG, Kashuk CS, Nouri N, Chakravarti A. Genome-wide association study and mouse model identify interaction between RET and EDNRB pathways in Hirschsprung disease. Nat Genet. 2002; 32:237–244.10.1038/ng998 [PubMed: 12355085]

Chai Y, Jiang X, Ito Y, Bringas P, Han J, Rowitch DH, Soriano P, McMahon AP, Sucov HM. Fate of the mammalian cranial neural crest during tooth and mandibular morphogenesis. Development. 2000; 127:1671–1679. [PubMed: 10725243]

Danielian PS, Muccino D, Rowitch DH, Michael SK, McMahon AP. Modification of gene activity in mouse embryos in utero by a tamoxifen-inducible form of Cre recombinase. Curr Biol. 1998; 8:1323–1326. [PubMed: 9843687]

D'Autréaux F, Morikawa Y, Cserjesi P, Gershon MD. Hand2 is necessary for terminal differentiation of enteric neurons from crest-derived precursors but not for their migration into the gut or for formation of glia. Development. 2007; 134:2237–2249.10.1242/dev.003814 [PubMed: 17507395]

De Pontual L, Pelet A, Clement-Ziza M, Trochet D, Antonarakis SE, Attie-Bitach T, Beales PL, Blouin JL, Moal FDL, Dollfus H, Goossens M, Katsanis N, Touraine R, Feingold J, Munnich A, Lyonnet

S, Amiel J. Epistatic interactions with a common hypomorphic RET allele in syndromic Hirschsprung disease. Hum Mutat. 2007; 28:790–796.10.1002/humu.20517 [PubMed: 17397038]

Echelard Y, Epstein DJ, St-Jacques B, Shen L, Mohler J, McMahon JA, McMahon AP. Sonic hedgehog, a member of a family of putative signaling molecules, is implicated in the regulation of CNS polarity. Cell. 1993; 75:1417–1430.10.1016/0092-8674(93)90627-3 [PubMed: 7916661]

Echelard Y, Vassileva G, McMahon AP. Cis-acting regulatory sequences governing Wnt-1 expression in the developing mouse CNS. Dev Camb Engl. 1994; 120:2213–2224.

Fuchs S, Herzog D, Sumara G, Büchmann-Møller S, Civenni G, Wu X, Chrostek-Grashoff A, Suter U, Ricci R, Relvas JB, Brakebusch C, Sommer L. Stage-Specific Control of Neural Crest Stem Cell Proliferation by the Small Rho GTPases Cdc42 and Rac1. Cell Stem Cell. 2009; 4:236–247.10.1016/j.stem.2009.01.017 [PubMed: 19265663]

Furness, JB. The enteric nervous system. Blackwell Publishing; Malden, MA: 2006.

Gabriel SB, Salomon R, Pelet A, Angrist M, Amiel J, Fornage M, Attié-Bitach T, Olson JM, Hofstra R, Buys C, Steffann J, Munnich A, Lyonnet S, Chakravarti A. Segregation at three loci explains familial and population risk in Hirschsprung disease. Nat Genet. 2002; 31:89–93.10.1038/ng868 [PubMed: 11953745]

Garcia-Barceló MM, Fong P, Tang CS, Miao X, So M, Yuan Z, Li L, Guo W, Liu L, Wang B, Sun XB, Huang LM, Tou JF, Wong KKY, Ngan ESW, Lui VC, Cherny SS, Sham P, Tam PK. Mapping of a Hirschsprung's disease locus in 3p21. Eur J Hum Genet. 2008; 16:833–840.10.1038/ejhg.2008.18 [PubMed: 18285831]

Garcia-Barcelo MM, Tang CS, Ngan ES, Lui VC, Chen Y, So M, Leon TY, Miao X, Shum CK, Liu F, Yeung M, Yuan Z, Guo W, Liu L, Sun X, Huang L, Tou J, Song Y, Chan D, Cheung KMC, Wong KK, Cherny SS, Sham P, Tam PK. Genome-wide association study identifies NRG1 as a susceptibility locus for Hirschsprung's disease. Proc Natl Acad Sci. 2009; 106:2694–2699.10.1073/pnas.0809630105 [PubMed: 19196962]

Goldstein A, Hofstra R, Burns A. Building a brain in the gut: development of the enteric nervous system. Clin Genet. 2013; 83:307–316.10.1111/cge.12054 [PubMed: 23167617]

Gu JJ, Stegmann S, Gathy K, Murray R, Laliberte J, Ayscue L, Mitchell BS. Inhibition of T lymphocyte activation in mice heterozygous for loss of the IMPDH II gene. J Clin Invest. 2000; 106:599–606.10.1172/JCI8669 [PubMed: 10953035]

Gu JJ, Tolin AK, Jain J, Huang H, Santiago L, Mitchell BS. Targeted Disruption of the Inosine 5′-Monophosphate Dehydrogenase Type I Gene in Mice. Mol Cell Biol. 2003; 23:6702–6712.10.1128/MCB.23.18.6702-6712.2003 [PubMed: 12944494]

Gunter JH, Thomas EC, Lengefeld N, Kruger SJ, Worton L, Gardiner EM, Jones A, Barnett NL, Whitehead JP. Characterisation of inosine monophosphate dehydrogenase expression during retinal development: Differences between variants and isoforms. Int J Biochem Cell Biol. 2008; 40:1716–1728.10.1016/j.biocel.2007.12.018 [PubMed: 18295529]

Hara-Kaonga B, Gao YA, Havrda M, Harrington A, Bergquist I, Liaw L. Variable Recombination Efficiency in Responder Transgenes Activated by Cre Recombinase in the Vasculature. Transgenic Res. 2006; 15:101–106.10.1007/s11248-005-2541-8 [PubMed: 16475014]

Hendershot TJ, Liu H, Sarkar AA, Giovannucci DR, Clouthier DE, Abe M, Howard MJ. Expression of Hand2 is sufficient for neurogenesis and cell type-specific gene expression in the enteric nervous system. Dev Dyn. 2007; 236:93–105.10.1002/dvdy.20989 [PubMed: 17075884]

Hotta R, Anderson RB, Kobayashi K, Newgreen DF, Young HM. Effects of tissue age, presence of neurones and endothelin-3 on the ability of enteric neurone precursors to colonize recipient gut: implications for cell-based therapies. Neurogastroenterol Motil. 2010; 22:331–e86.10.1111/j.1365-2982.2009.01411.x [PubMed: 19775251]

Huang T, Liu Y, Huang M, Zhao X, Cheng L. Wnt1-cre-mediated Conditional Loss of Dicer Results in Malformation of the Midbrain and Cerebellum and Failure of Neural Crest and Dopaminergic Differentiation in Mice. J Mol Cell Biol. 2010; 2:152–163.10.1093/jmcb/mjq008 [PubMed: 20457670]

Jiang X, Iseki S, Maxson RE, Sucov HM, Morriss-Kay GM. Tissue Origins and Interactions in the Mammalian Skull Vault. Dev Biol. 2002; 241:106–116.10.1006/dbio.2001.0487 [PubMed: 11784098]

Jiang X, Rowitch DH, Soriano P, McMahon AP, Sucov HM. Fate of the mammalian cardiac neural crest. Development. 2000; 127:1607–1616. [PubMed: 10725237]

Kapur RP. Colonization of the murine hindgut by sacral crest-derived neural precursors: experimental support for an evolutionarily conserved model. Dev Biol. 2000; 227:146–155.10.1006/dbio.2000.9886 [PubMed: 11076683]

Kapur RP, Livingston R, Doggett B, Sweetser DA, Siebert JR, Palmiter RD. Abnormal microenvironmental signals underlie intestinal aganglionosis in dominant megacolon mutant mice. Dev Biol. 1996; 174:360–369.10.1006/dbio.1996.0080 [PubMed: 8631507]

Kapur RP, Sweetser DA, Doggett B, Siebert JR, Palmiter RD. Intercellular signals downstream of endothelin receptor-B mediate colonization of the large intestine by enteric neuroblasts. Development. 1995; 121:3787–3795. [PubMed: 8582288]

Lake JI, Heuckeroth RO. Enteric nervous system development: migration, differentiation, and disease. Am J Physiol - Gastrointest Liver Physiol. 2013; 305:G1–G24.10.1152/ajpgi.00452.2012 [PubMed: 23639815]

Lake JI, Tusheva OA, Graham BL, Heuckeroth RO. Hirschsprung-like disease is exacerbated by reduced de novo GMP synthesis. J Clin Invest. 2013; 123:4875–4887.10.1172/JCI69781 [PubMed: 24216510]

Lee HY, Kleber M, Hari L, Brault V, Suter U, Taketo MM, Kemler R, Sommer L. Instructive Role of Wnt/β-Catenin in Sensory Fate Specification in Neural Crest Stem Cells. Science. 2004; 303:1020–1023.10.1126/science.1091611 [PubMed: 14716020]

Lei J, Howard MJ. Targeted deletion of Hand2 in enteric neural precursor cells affects its functions in neurogenesis, neurotransmitter specification and gangliogenesis, causing functional aganglionosis. Development. 2011; 138:4789–4800.10.1242/dev.060053 [PubMed: 21989918]

Lennon VA. The case for a descriptive generic nomenclature: clarification of immunostaining criteria for PCA-1, ANNA-1, and ANNA-2 autoantibodies. Neurology. 1994; 44:2412–2415. [PubMed: 7991144]

Lewandoski M, Meyers EN, Martin GR. Analysis of Fgf8 Gene Function in Vertebrate Development. Cold Spring Harb Symp Quant Biol. 1997; 62:159–168.10.1101/SQB.1997.062.01.021 [PubMed: 9598348]

Lin AE, Singh KE, Strauss A, Nguyen S, Rawson K, Kimonis VE. An additional patient with mycophenolate mofetil embryopathy: Cardiac and facial analyses. Am J Med Genet A. 201110.1002/ajmg.a.33934

Maka M, Claus Stolt C, Wegner M. Identification of Sox8 as a modifier gene in a mouse model of Hirschsprung disease reveals underlying molecular defect. Dev Biol. 2005; 277:155–169.10.1016/j.ydbio.2004.09.014 [PubMed: 15572147]

Matsuoka T, Ahlberg PE, Kessaris N, Iannarelli P, Dennehy U, Richardson WD, McMahon AP, Koentges G. Neural crest origins of the neck and shoulder. Nature. 2005; 436:347–355. [PubMed: 16034409]

McLeod MJ. Differential staining of cartilage and bone in whole mouse fetuses by alcian blue and alizarin red S. Teratology. 1980; 22:299–301.10.1002/tera.1420220306 [PubMed: 6165088]

Mundell NA, Plank JL, LeGrone AW, Frist AY, Zhu L, Shin MK, Southard-Smith EM, Labosky PA. Enteric nervous system specific deletion of Foxd3 disrupts glial cell differentiation and activates compensatory enteric progenitors. Dev Biol. 2012; 363:373–387.10.1016/j.ydbio.2012.01.003 [PubMed: 22266424]

Nagai M, Natsumeda Y, Weber G. Proliferation-linked Regulation of Type II IMP Dehydrogenase Gene in Human Normal Lymphocytes and HL-60 Leukemic Cells. Cancer Res. 1992; 52:258–261. [PubMed: 1345808]

Natarajan D, Grigoriou M, Marcos-Gutierrez CV, Atkins C, Pachnis V. Multipotential progenitors of the mammalian enteric nervous system capable of colonising aganglionic bowel in organ culture. Development. 1999; 126:157–168. [PubMed: 9834195]

Obermayr F, Hotta R, Enomoto H, Young HM. Development and developmental disorders of the enteric nervous system. Nat Rev Gastroenterol Hepatol. 2013; 10:43–57.10.1038/nrgastro.2012.234 [PubMed: 23229326]

Okamura Y, Saga Y. Notch signaling is required for the maintenance of enteric neural crest progenitors. Development. 2008; 135:3555–3565.10.1242/dev.022319 [PubMed: 18832397]

Olaopa M, Zhou H, Snider P, Wang J, Schwartz RJ, Moon AM, Conway SJ. Pax3 is essential for normal cardiac neural crest morphogenesis but is not required during migration nor outflow tract septation. Dev Biol. 2011; 356:308–322.10.1016/j.ydbio.2011.05.583 [PubMed: 21600894]

Porras D, Brown CB. Temporal–spatial ablation of neural crest in the mouse results in cardiovascular defects. Dev Dyn. 2008; 237:153–162.10.1002/dvdy.21382 [PubMed: 18058916]

Preibisch S, Saalfeld S, Tomancak P. Globally optimal stitching of tiled 3D microscopic image acquisitions. Bioinformatics. 2009; 25:1463–1465.10.1093/bioinformatics/btp184 [PubMed: 19346324]

R. Core Team. R: A Language and Environment for Statistical Computing. Vienna, Austria: 2012.

Rothman TP, Le Douarin NM, Fontaine-Pérus JC, Gershon MD. Colonization of the bowel by neural crest-derived cells re-migrating from foregut backtransplanted to vagal or sacral regions of host embryos. Dev Dyn Off Publ Am Assoc Anat. 1993; 196:217–233.10.1002/aja.1001960308

Schindelin J, Arganda-Carreras I, Frise E, Kaynig V, Longair M, Pietzsch T, Preibisch S, Rueden C, Saalfeld S, Schmid B, Tinevez JY, White DJ, Hartenstein V, Eliceiri K, Tomancak P, Cardona A. Fiji: an open-source platform for biological-image analysis. Nat Methods. 2012; 9:676–682.10.1038/nmeth.2019 [PubMed: 22743772]

Schneider CA, Rasband WS, Eliceiri KW. NIH Image to ImageJ: 25 years of image analysis. Nat Methods. 2012; 9:671–675.10.1038/nmeth.2089 [PubMed: 22930834]

Senda M, Natsumeda Y. Tissue-differential expression of two distinct genes for human IMP dehydrogenase (E.C.1.1.1.205). Life Sci. 1994; 54:1917–1926.10.1016/0024-3205(94)90150-3 [PubMed: 7910933]

Simpson MJ, Zhang DC, Mariani M, Landman KA, Newgreen DF. Cell proliferation drives neural crest cell invasion of the intestine. Dev Biol. 2007; 302:553–568.10.1016/j.ydbio.2006.10.017 [PubMed: 17178116]

Smith CA, McClive PJ, Hudson Q, Sinclair AH. Male-specific cell migration into the developing gonad is a conserved process involving PDGF signalling. Dev Biol. 2005; 284:337–350.10.1016/j.ydbio.2005.05.030 [PubMed: 16005453]

Srinivas S, Watanabe T, Lin CS, William CM, Tanabe Y, Jessell TM, Costantini F. Cre reporter strains produced by targeted insertion of EYFP and ECFP into the ROSA26 locus. BMC Dev Biol. 2001; 1:4–4.10.1186/1471-213X-1-4 [PubMed: 11299042]

Stratman JL, Barnes WM, Simon TC. Universal PCR genotyping assay that achieves single copy sensitivity with any primer pair. Transgenic Res. 2003; 12:521–522.10.1023/A:1024225408961 [PubMed: 12885173]

Truett GE, Heeger P, Mynatt RL, Truett AA, Walker JA, Warman ML. Preparation of PCR-quality mouse genomic DNA with hot sodium hydroxide and tris (HotSHOT). BioTechniques. 2000; 29:52, 54. [PubMed: 10907076]

Uesaka T, Enomoto H. Neural precursor death is central to the pathogenesis of intestinal aganglionosis in ret hypomorphic mice. J Neurosci. 2010; 30:5211–5218.10.1523/JNEUROSCI.6244-09.2010 [PubMed: 20392943]

Van de Putte T, Francis A, Nelles L, van Grunsven LA, Huylebroeck D. Neural crest-specific removal of Zfhx1b in mouse leads to a wide range of neurocristopathies reminiscent of Mowat-Wilson syndrome. Hum Mol Genet. 2007; 16:1423–1436.10.1093/hmg/ddm093 [PubMed: 17478475]

Vooijs M, Jonkers J, Berns A. A highly efficient ligand-regulated Cre recombinase mouse line shows that LoxP recombination is position dependent. EMBO Rep. 2001; 2:292–297.10.1093/embo-reports/kve064 [PubMed: 11306549]

Wang J, Zeevi A, Webber S, Girnita DM, Addonizio L, Selby R, Hutchinson IV, Burckart GJ. A Novel Variant L263F in Human Inosine 5′-Monophosphate Dehydrogenase 2 Is Associated with Diminished Enzyme Activity. Pharmacogenet Genomics. 2007; 17:283–290.10.1097/FPC.0b013e328012b8cf [PubMed: 17496727]

Wang S, Liu B, Tao HW, Xia K, Zhang LI. A Genetic Strategy for Stochastic Gene Activation with Regulated Sparseness (STARS). PLoS ONE. 2009; 4:e4200.10.1371/journal.pone.0004200 [PubMed: 19145242]

Young HM, Bergner AJ, Anderson RB, Enomoto H, Milbrandt J, Newgreen DF, Whitington PM. Dynamics of neural crest-derived cell migration in the embryonic mouse gut. Dev Biol. 2004; 270:455–473.10.1016/j.ydbio.2004.03.015 [PubMed: 15183726]

Young, Hm; Newgreen, D. Enteric neural crest-derived cells: Origin, identification, migration, and differentiation. Anat Rec. 2001; 262:1–15.10.1002/1097-0185(20010101)262:1<1::AID-AR1006>3.0.CO;2-2 [PubMed: 11146424]

Zehir A, Hua LL, Maska EL, Morikawa Y, Cserjesi P. Dicer is required for survival of differentiating neural crest cells. Dev Biol. 2010; 340:459–467.10.1016/j.ydbio.2010.01.039 [PubMed: 20144605]

Zheng B, Sage M, Sheppeard EA, Jurecic V, Bradley A. Engineering Mouse Chromosomes with Cre-loxP: Range, Efficiency, and Somatic Applications. Mol Cell Biol. 2000; 20:648–655.10.1128/MCB.20.2.648-655.2000 [PubMed: 10611243]

Zimmermann AG, Spychala J, Mitchell BS. Characterization of the human inosine-5′-monophosphate dehydrogenase type II gene. J Biol Chem. 1995; 270:6808–6814.10.1074/jbc.270.12.6808 [PubMed: 7896827]

Zimmermann A, Gu JJ, Spychala J, Mitchell BS. Inosine monophosphate dehydrogenase expression: Transcriptional regulation of the type I and type II genes. Adv Enzyme Regul. 1996; 36:75–84.10.1016/0065-2571(95)00012-7 [PubMed: 8869741]

Highlights

- *Impdh2* is required for enteric nervous system, heart, and facial bone development.
- *Impdh1* cannot substitute for *Impdh2*.
- Cell autonomous *de novo* guanine nucleotide synthesis is essential for neural crest.

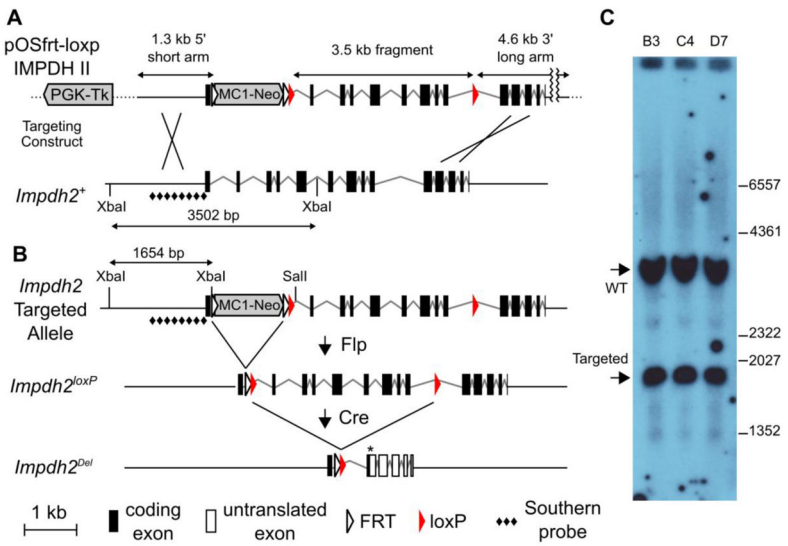

Figure 1. Production and structure of the *Impdh2*^{loxP} and *Impdh2*^{Del} alleles

(**A**) The *Impdh2* targeting construct, shown above the corresponding wild-type *Impdh2* locus, contains *loxP* sequences (red triangles) in intron 1 and intron 9 while *FRT* sequences (hollow triangles) flank a *MC1-Neo* cassette immediately preceding the first *loxP* site. Flp-mediated recombination excises the *MC1-Neo* cassette (**B**) from the targeted allele to produce the conditional *Impdh2*^{loxP} allele. Cre-mediated recombination produces the *Impdh2*^{Del} allele, which results in a frameshift (asterisk) and premature termination codon in the exon 3′ to the recombination site. After CRE-mediated DNA recombination, the IMPDH catalytic domain will be not be produced. (**A** and **B**): Intergenic restriction sites and those not resolved by Southern blot are omitted for clarity. (**C**) Southern blot of DNA from three PCR-positive ES cell clones digested with XbaI showing expected bands at 3502 bp (WT) and 1654 bp (targeted).

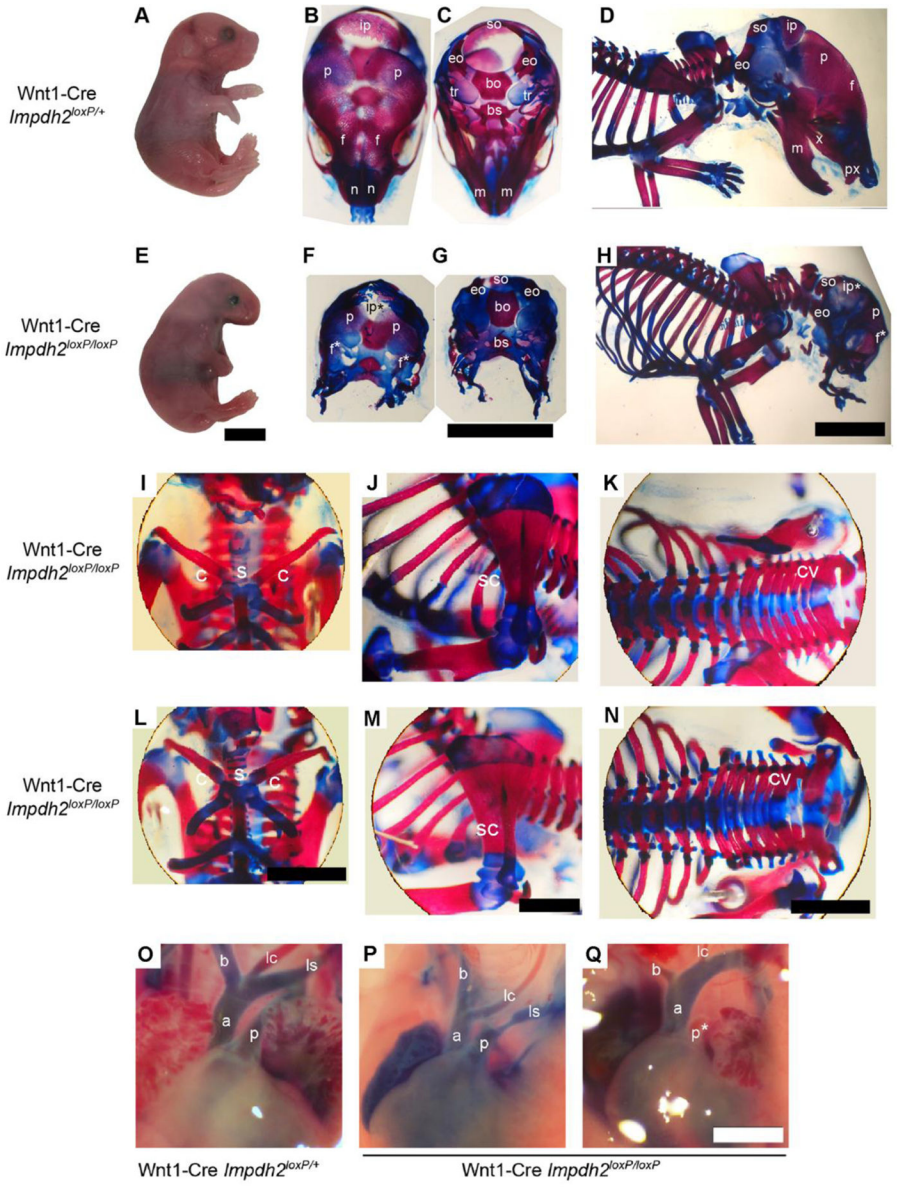

Figure 2. *Impdh2* deletion by Wnt1-Cre results in craniofacial and cardiac defects at term

At embryonic day 18.5 (E18.5), (**A, E**) Wnt1-Cre *Impdh2*$^{loxP/loxP}$ fetuses lack a jaw, external ear, or any mineralized bone in the anterior head. (**B, F**) superior, (**C, G**) inferior, and (**D, H**) lateral views of bone and cartilage stained skulls show that Wnt1-Cre *Impdh2*$^{loxP/loxP}$ fetuses have missing or severely reduced neural-crest derived skeletal structures of the head, including most structures anterior to the parietal and basiosphenoid bones as well as the neural crest derived interparietal bone and tympanic rings. In contrast, the sternum, clavicle (I,L), scapular spine (J,M), and spinous processes of the cervical vertebrae (K,N) appear grossly normal. bo = basiooccipital bone, bs = basisphenoid bone, eo = exooccipital bone, f = frontal bone, m = mandible, n = nasal bone, p = parietal bone, px = premaxilla, ip = interparietal bone, so = supraoccipital bone, tr = tymanic ring, x = maxilla, c = clavicle, s = sternum, sc = scapular spine, cv = cervical vertebrae, * = remnant or

abnormal structure. Scale bars in panels A–H = 5 mm. Scale bars in panel I-N = 2.5 mm. Injection of ink into the ventricles of control *Wnt1-Cre Impdh2*$^{loxP/+}$ hearts (O) reveals normal anatomy of the great arteries. *Wnt1-Cre Impdh2*$^{loxP/loxP}$ hearts (P, Q) show representative malformations of the great vessels and outflow tract: P shows an interrupted aortic arch, where the left subclavian (ls) arises from the pulmonary artery instead of the aorta. In Q, the pulmonary artery fails to label with ink despite ink injection into the right ventricle, indicating pulmonic stenosis or atresia. a = aorta, p = pulmonary artery, b = brachiocephalic trunk, lc = left common carotid artery, ls = left subclavian artery, p* = atretic pulmonary artery. Scale bar = 2 mm.

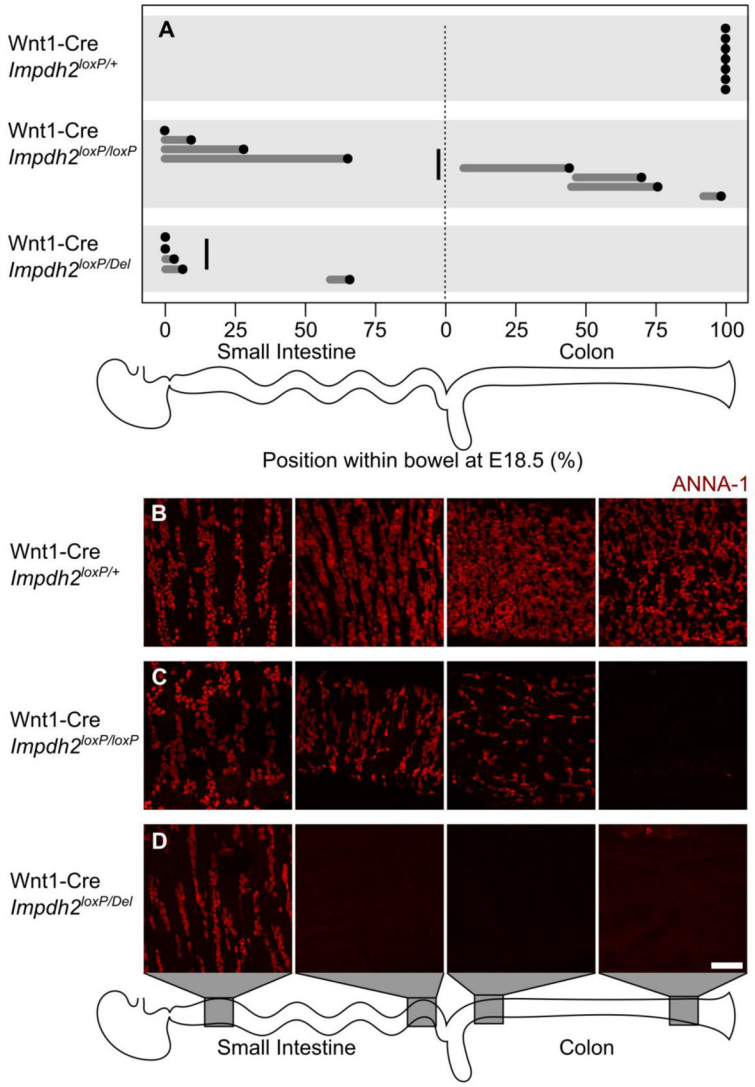

Figure 3. *Impdh2* deletion by Wnt1-Cre causes highly penetrant aganglionosis of variable length at term

(**A**) At E18.5, all Wnt1-Cre *Impdh2*$^{loxP/+}$ bowels are fully colonized by neurons, while Wnt1-Cre *Impdh2*$^{loxP/loxP}$ and Wnt1-Cre *Impdh2*$^{loxP/Del}$ intestines demonstrate distal aganglionosis reminiscent of Hirschsprung disease. Proximal to aganglionic bowel there is a hypoganglionic transition zone and eventually, in many cases, regions of relatively normal appearing proximal bowel. Each dot and line represents a separate fetus. Dots = position of the most caudal enteric neuron in each intestine, grey lines = hypoganglionic regions, vertical lines = mean positions of the most caudal ENCDC. (**B**) ANNA–1 (anti-HuC/HuD) staining of enteric neuron somata reveals that Wnt1-Cre *Impdh2*$^{loxP/+}$ contain a dense network of enteric neurons throughout the bowel. (**C–D**) Conditional knockout genotypes contain variable regions of distal aganglionic bowel. (C) Shows aganglionic distal colon, hypoganglionic proximal colon and relatively normal regions of the ENS in the proximal small intestine. (D) Shows aganglionic colon and distal small bowel with a relatively normal

appearing enteric neuron density in proximal small bowel. ANNA–1 photomicrographs are maximum intensity projections of 20 micron-thick volumes. Scale bar = 100 μm.

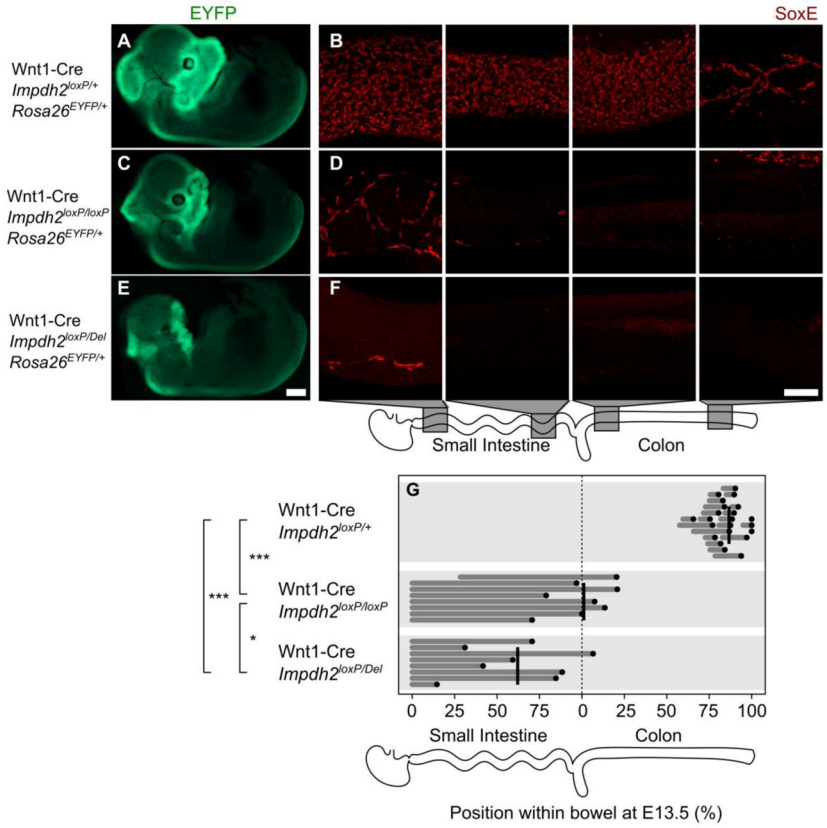

Figure 4. *Impdh2* conditional knockout fetuses have cranial neural crest and ENCDC abnormalities at E13.5

(**A, C, E**) EYFP-positive neural crest derivatives have migrated to the anterior head in all genotypes, but in (**C**) Wnt1-Cre *Rosa26*^{EYFP} *Impdh2*$^{loxP/loxP}$ fetuses, EYFP-positive tissue is reduced in size and has not fused at the ventral midline where the medial nasal prominence exists in *Impdh2*$^{loxP/+}$ fetuses. In (**E**) Wnt1-Cre *Rosa26*^{EYFP} *Impdh2*$^{loxP/Del}$ fetuses, EYFP-positive tissue is still present anterolaterally but does not form recognizable branchial arch structures. Scale bar = 1 mm. In (**B**) control bowel, SOXE-positive enteric neural crest-derived cells (ENCDCs) have colonized almost the entire bowel and have accumulated to a high density in colonized regions (small intestine and proximal colon). In (**D**) Wnt1-Cre *Impdh2*$^{loxP/loxP}$ and (**F**) *Impdh2*$^{loxP/Del}$ intestine, colonized regions are both significantly shorter and contain fewer cells, indicating a profound inability for ENCDCs to efficiently populate the intestine. Scale bar = 100 μm. Measurements (**G**) of colonization extent as well as colonized regions of bowel containing an unusually low ENCDC density reveal that Wnt1-Cre *Impdh2*$^{loxP/Del}$ intestine has a significantly worse colonization defect than Wnt1-Cre *Impdh2*$^{loxP/loxP}$. Each dot and line represents a separate fetus. Dots = position of the most caudal ENCDC in each intestine as indicated by EYFP expression in *Rosa26*^{EYFP} bowels or SOXE staining in *Rosa26 WT* bowels. Grey lines = regions of low ENCDC density. Vertical lines = mean positions of the most caudal ENCDC. * = $P < .05$, *** = $P < .001$ by Welch's t-test on the most-caudal ENCDC positions.

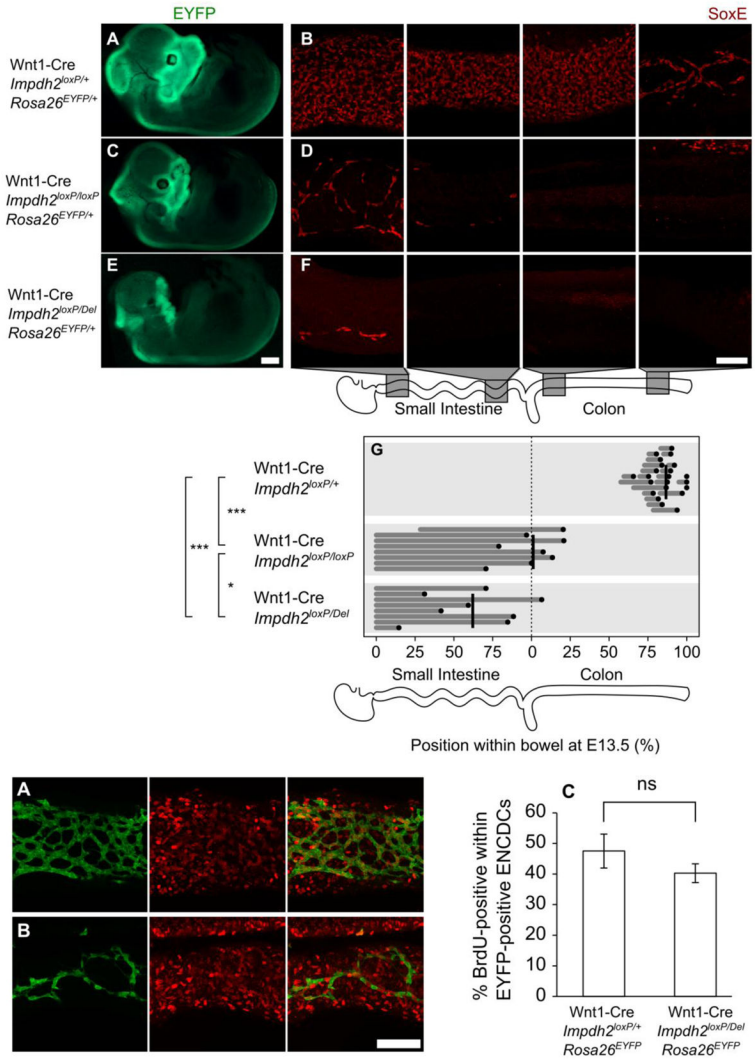

Figure 5. BrdU incorporation in ENCDCs of *Impdh2* conditional knockout fetuses

(**A**) Immediately behind the migration wavefront in E13.5 Wnt1-Cre *Rosa26*^{EYFP} *Impdh2*$^{loxP/+}$ bowel, many EYFP-positive ENCDCs (green) incorporate bromodeoxyuridine (BrdU, red and merge). (**B**) At this time point, very few ENCDCs are present in the small intestine of Wnt1-Cre *Rosa26*^{EYFP} *Impdh2*$^{loxP/Del}$ fetuses. Scale bar = 100 μm. Pictures are maximum intensity projections of 12 μm-thick volumes. (**C**) Quantification of BrdU incorporating nuclei within the EYFP-marked ENCDC population does not demonstrate a significant difference in BrdU incorporation between *Impdh2*$^{loxP/+}$ (N = 5) and *Impdh2*$^{loxP/Del}$ (N = 4) genotypes. Note that different regions of the bowel are being compared, since each contains the migration wavefront in its respective genotype. ns = not significant by pooled-variance t-test. Error bars are s.e.m.

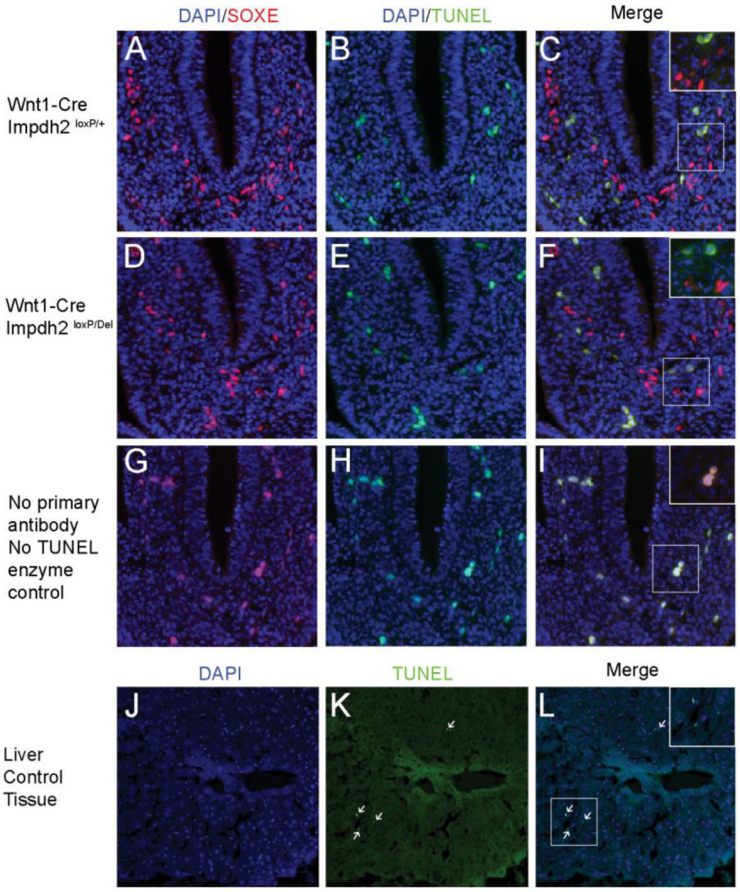

Figure 6. TUNEL labeling of E9.5 vagal neural crest progenitors in *Impdh2* conditional knockout embryos

Vagal neural crest progenitors labeled with SOXE are seen entering the foregut in both control and *Impdh2* conditional knockout embryos, with no significant TUNEL labeling detected in mice of either genotype (A–F). Autofluorescent nucleated red blood cells are observed in all samples in the absence of primary antibody or TUNEL reagents (G–I). Apoptotic TUNEL-labeled cells are readily detected in positive control liver samples (J–L).

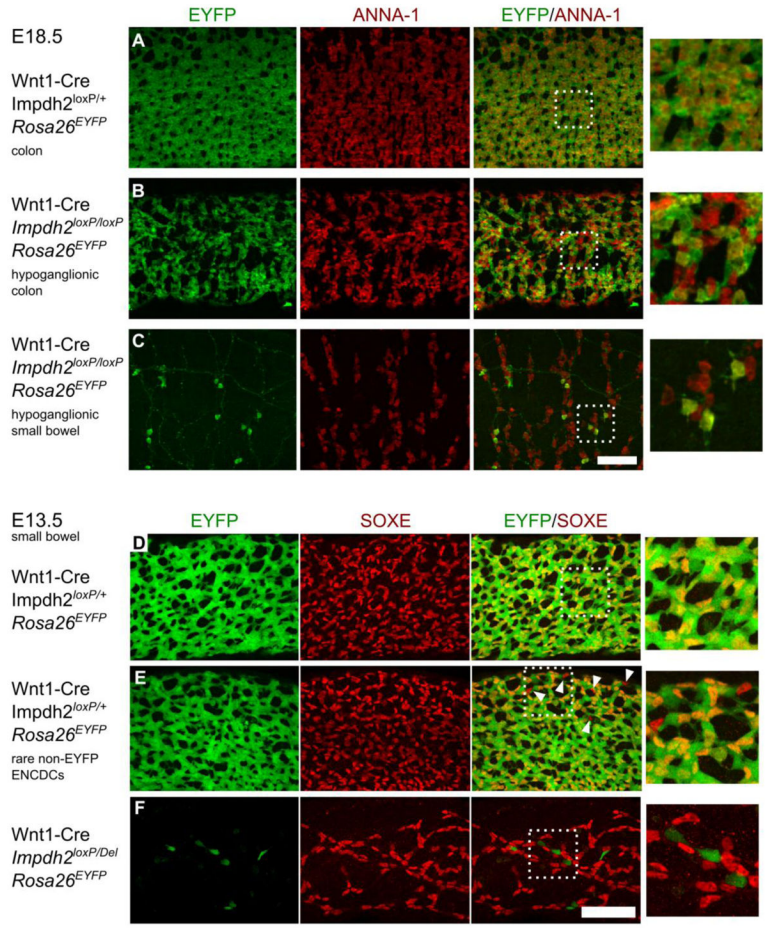

Figure 7. Remaining enteric neurons and ENCDCs in *Impdh2* conditional knockouts display incomplete recombination

In (**A**) morphologically normal colon of Wnt1-Cre *Impdh2*$^{loxP/+}$ *Rosa26*^{EYFP} control fetuses, all ANNA–1-positive (anti-HuC/HuD, red) enteric neurons are EYFP-positive (green) at E18.5, demonstrating that under normal circumstances Wnt1-Cre efficiently recombines the ancestors of essentially all ENCDCs. In (**B**) the hypoganglionic colon of one Wnt1-Cre *Rosa26*^{EYFP} *Impdh2*$^{loxP/loxP}$ fetus and (**C**) the small bowel of another, more severely affected fetus with aganglionosis extending into the small bowel (**C**), many enteric neurons are not EYFP-positive, and the degree of incomplete labeling varies. (**D–F**) A similar phenomenon is already visible in the small intestine at E13.5. ENCDCs (SOXE-positive, red) are uniformly EYFP-positive (green) in (**D**) most control Wnt1-Cre *Rosa26*^{EYFP} *Impdh2*$^{loxP/+}$ bowel. In (**E**), the individual SOXE-positive, EYFP-negative cells (identified by arrowheads) are the only examples of incomplete recombination found in the Wnt1-Cre *Rosa26*^{EYFP} *Impdh2*$^{loxP/+}$ genotype, likely representing a clone of ENCDCs derived from a rare neural crest cell that escaped recombination. In contrast, many SOXE-positive ENCDCs are EYFP-negative (**F**) in Wnt1-Cre *Rosa26*^{EYFP} *Impdh2*$^{loxP/Del}$ bowel. Dashed boxes = magnified insets. All scale bars = 100 μm. All photomicrographs are maximum intensity projections of 20 micron-thick volumes.